Convective Cells and Blob Control in a Simple Magnetized Plasma

C. Theiler,[1] I. Furno,[1] J. Loizu,[1] and A. Fasoli[1]

[1]*Ecole Polytechnique Fédérale de Lausanne (EPFL), Centre de Recherches en Physique des Plasmas, Association Euratom-Confédération Suisse, CH-1015 Lausanne, Switzerland*

(Received 4 November 2011; published 10 February 2012)

Blob control by creating convective cells using biased electrodes is demonstrated in simple magnetized toroidal plasmas. A two-dimensional array of electrodes is installed on a metal limiter to obtain different biasing schemes. Detailed two-dimensional measurements across the magnetic field reveal the formation of a convective cell, which shows a high degree of uniformity along the magnetic field. Depending on the biasing scheme, radial and vertical blob velocities can be varied significantly. A high level of cross-field currents limits the achievable potential variations to values well below the applied bias voltage. Furthermore, the strongest potential variations are not induced along the biased flux tube, but at a position shifted in the direction of plasma flows.

DOI: 10.1103/PhysRevLett.108.065005 PACS numbers: 52.35.Ra, 52.25.Fi, 52.25.Xz

Understanding and handling turbulent dynamics in the edge of magnetized laboratory plasmas is critical for magnetic fusion research. Edge turbulence in fusion devices influences the overall plasma confinement, heat fluxes on the divertor plates, as well as processes like impurity production and influx, main chamber recycling, tritium retention, and helium ash removal [1–3]. It has been proposed that inducing convective cells could serve as a method to modify edge turbulence, possibly increase the Scrape-Off Layer (SOL) width and reduce divertor heat loads [4]. Such ideas have been tested in several tokamaks [5–8] by applying toroidal or poloidal asymmetric biasing. While clear effects on radial flows and density and heat flux profiles could be demonstrated, the structure of induced convective cells in the plane perpendicular to the magnetic field remains unclear due to the lack of two-dimensional (2D) measurements.

In this Letter, we investigate the basic mechanisms governing the formation of convective cells and their effect on turbulent structures using detailed 2D measurements. An array of 3×8 biasing electrodes is used to produce modifications of time-averaged profiles that reveal features of convective cells. Depending on the biasing scheme, we demonstrate that both radial and vertical velocities of turbulent structures are significantly modified. We show that the effect of biasing on the time-averaged profiles is fairly uniform along the magnetic field. The magnitude of the induced potential structures is limited by cross-field currents and its position is shifted with respect to the biased flux tube in the direction of plasma flows.

Experiments are conducted in the simple magnetized toroidal device TORPEX [9] (major radius $R = 1$ m, minor radius $a = 0.2$ m), which is dedicated to the basic study of turbulence and transport. With open field lines and curvature driven instabilities, important aspects of SOL turbulence are present in TORPEX. At the same time, full access with probes is possible due to relatively low values of density and temperature, allowing for detailed measurements along and across the magnetic field. Plasmas are produced and sustained by microwaves in the electron cyclotron range of frequencies and confined by a dominant toroidal magnetic field B_ϕ, on which a small vertical component B_z is superimposed. This leads to helical field lines that wind around the torus and intercept the vacuum vessel at the bottom and the top, as sketched in Fig. 1. The dominant instability in TORPEX depends on the value of the vertical field component. By increasing B_z, a transition from $k_\parallel \neq 0$ modes to modes with $k_\parallel = 0$ is observed [10], where $k_\parallel$ is the wave number along the magnetic field. Using global, three-dimensional fluid simulations, it has recently been demonstrated that this corresponds to a transition from a turbulent regime dominated by resistive interchange waves to one dominated by ideal interchange waves [11]. In the present experiments, we use $B_\phi \approx 76$ mT and $B_z \approx 1.55$ mT, which falls in the ideal interchange regime. For sufficiently low values of

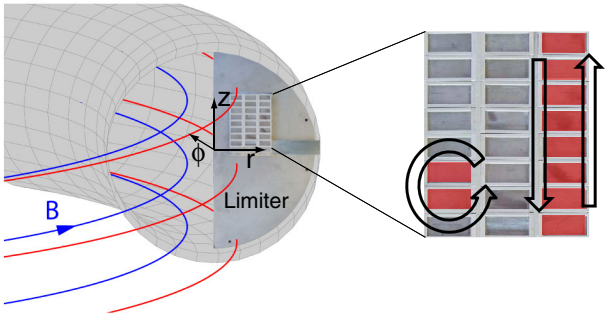

FIG. 1 (color online). Sketch of the TORPEX vacuum vessel and the electrodes installed on a conducting limiter. Examples of magnetic field lines and the coordinate system are also shown. An enlarged view of the electrodes is shown at the right. Shaded areas indicate examples of positively biased electrodes and arrows show the expected flow pattern.

injected microwave power, vertically elongated plasmas are generated. By adjusting the value of B_ϕ, these plasmas can be positioned towards the high-field side (HFS). Hydrogen at a pressure of $\approx 2 \times 10^{-4}$ mbar is used as working gas. Electron density and temperature are $\lesssim 10^{16}$ m^{-3} and $\lesssim 8$ eV, respectively. Plasma production is limited to the HFS. The ideal interchange wave develops on the low-field side (LFS) of the profiles around the position of maximum pressure gradient and intermittently ejects plasma filaments (blobs) radially outwards into a region with negligible plasma production. These blobs are structures of enhanced density relative to the background plasma that are elongated along the magnetic field but are localized in the perpendicular plane [12,13]. Their formation [14–16], subsequent propagation [17–19], and associated transport [20], driven by ∇B and curvature induced polarization, have been extensively studied in this scenario. For the plasmas investigated here, blob polarization and radial velocity is limited both by parallel currents to the wall and cross-field currents inside the plasma [17–19].

A grounded stainless steel limiter is installed in the blob propagation region and an array of 3×8 stainless steel electrodes is mounted on its surface, as sketched in Fig. 1. Each rectangular electrode with a surface of 2 cm $\times$ 0.9 cm is installed on an isolating support. This setup protrudes from the limiter by ≈ 8 mm. Each of the 24 electrodes can be biased individually and its current can be measured. Measurements are mainly performed with the Langmuir probe (LP) arrays SLP and HEXTIP [21]. SLP is a vertical array of 8 LPs that can be moved radially and rotated in the toroidal direction. Besides measuring ion saturation current I_{sat} or floating potential V_{fl}, it can be operated in swept mode to measure the time-averaged current-voltage (I-V) characteristics. HEXTIP is a 2D array of 86 LPs that cover the whole plasma poloidal cross section and provide I_{sat} or V_{fl} measurements. HEXTIP is displaced toroidally by 90° from the limiter, in the clockwise direction when the torus is seen from top. SLP lies between limiter and HEXTIP, at 55° from the limiter.

In Fig. 2, we show time-averaged profiles of (a) I_{sat} and (b) V_{pl} measured with SLP during a 800 μs phase of the discharge, the "bias off" phase, in which all electrodes are grounded. In Fig. 2(b), the $\mathbf{E} \times \mathbf{B}$ velocity field deduced from V_{pl} is also plotted. As typical for these plasmas [14], the $\mathbf{E} \times \mathbf{B}$ drift is directed mainly downwards on the HFS and upwards on the LFS of the I_{sat} profile. A V_{pl} structure is observed at the LFS already during the bias off phase. This is an indication for steady-state radial flows as reported also from tokamaks [22]. During a subsequent 800 μs phase of the discharges, the "bias on" phase, we apply a voltage of +40 V to the pair of electrodes that is represented by black rectangles at their field line-mapped position in the SLP plane in Figs. 2(c) and 2(d). These electrodes draw a total current of ≈ -30 mA from the plasma. Figure 2(c) shows the relative change in I_{sat}

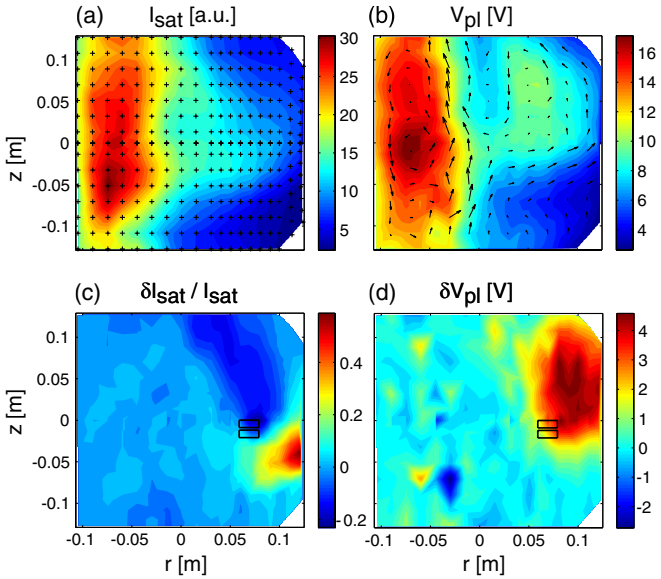

FIG. 2 (color online). Profiles of (a) I_{sat} and (b) V_{pl} measured with SLP. Measurement points are indicated by the +'s in (a). Vectors in (b) represent the $\mathbf{E} \times \mathbf{B}$ velocity. (c) and (d) show the relative changes in I_{sat} and the absolute changes in V_{pl} induced by biasing the indicated set of electrodes to +40 V.

and (d) the change in V_{pl} due to the bias (we use here δ to indicate the difference of a time averaged quantity between the bias on and the bias off phase). We observe characteristics of a convective cell, namely, a positive structure in δV_{pl} and changes in I_{sat} up to 60% that are consistent with a counterclockwise rotation around the δV_{pl} structure. Less expected features are the relatively large size of the δV_{pl} structure and its vertical and radial displacement with respect to the biased flux tube. Further, the peak value of δV_{pl} of ≈ 4 V, which corresponds to ~ 1.8 times the electron temperature in that region, is well below the applied bias of +40 V. We discuss these features in more detail later and focus now on the effect of biasing on blob motion.

To modify both vertical and radial blob velocities, we apply a bias of +40 V to two different sets of electrodes during the bias on phase. These are indicated by black rectangles at their position in the SLP plane in Figs. 3 and 4. SLP is operated in I_{sat} mode and displaced radially in between reproducible discharges. Conditional average sampling (CAS) [15,16] with a HEXTIP signal as reference probe is applied to obtain the average, 2D evolution of blob propagation. Figures 3 and 4 show successive time frames of blob propagation from CAS analysis. $t = 0$ corresponds to the time when blobs are detected at the reference probe. Color plots show results for the bias on phase, while blob I_{sat} contours during the bias off phase are shown in white. In Fig. 3, a vertical stripe of electrodes is used during the bias on phase. Early in time, the average blob evolution is very similar in the bias on and bias off phase. Later on, as anticipated, the blob is swept strongly

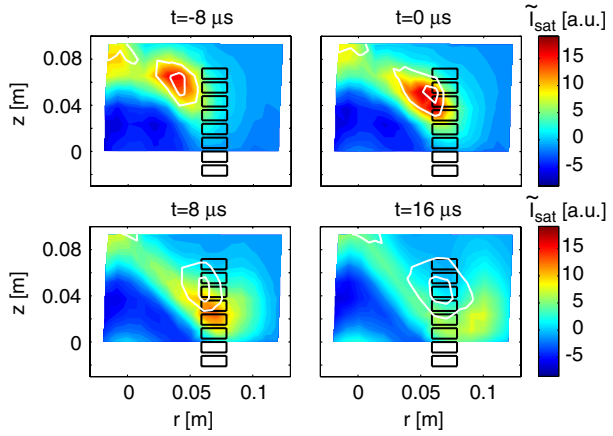

FIG. 3 (color online). Conditionally averaged blob propagation (I_{sat} fluctuations) for the case where a vertical stripe of electrodes is biased to +40 V (color plots). For comparison, the white contours indicate the results of the same analysis when all electrodes are grounded.

downwards due to the applied bias. In the time interval $[-8\ \mu s, 8\ \mu s]$, the blob vertical velocity changes from $v_z \approx -700\ \mathrm{ms}^{-1}$ to $v_z \approx -2100\ \mathrm{ms}^{-1}$ due to the biasing. For the case shown in Fig. 4, a set of four electrodes is used to induce a counterclockwise rotating cell. As expected, blobs passing below this set of electrodes are radially accelerated with respect to the unbiased case. In the time interval $[8\ \mu s, 16\ \mu s]$, the blob radial velocity increases from $v_r \approx 1200\ \mathrm{ms}^{-1}$ to $v_r \approx 2200\ \mathrm{ms}^{-1}$ due to the biasing. These examples demonstrate that biasing allows influencing both vertical and radial blob velocities. The observed changes in blob velocity are indeed in quantitative agreement with the convective motion deduced from the measured profile of δV_{pl}. As already seen in Fig. 2(d), the shape of the δV_{pl} profile can, however, differ from that expected from the bias configuration. We note that the reduction in time of the blob amplitude apparent from

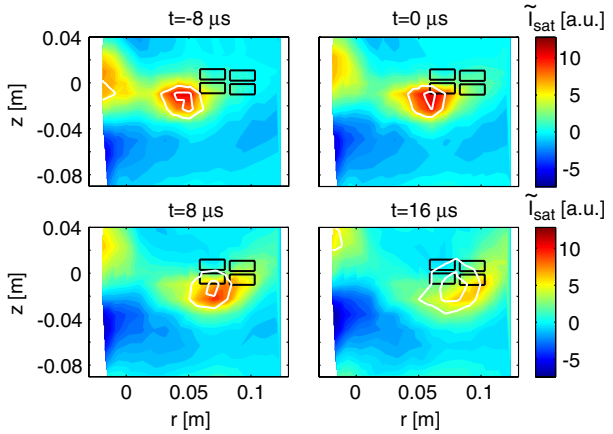

FIG. 4 (color online). The same as Fig. 3 for a different biasing pattern.

Figs. 3 and 4 is a general feature of CAS [16] and is also observed in the absence of biasing.

So far, we have focused on the effect of biasing in a given cross section, toroidally separated by ≈ 1 m from the limiter. We investigate now the biasing effect dependence upon the toroidal position. To this end, we compare measurements with HEXTIP at 90° from the limiter with measurements directly on the limiter. Similarly to previous experiments, during the bias on phase, we apply a voltage of +40 V to a pair of electrodes and ground them during the bias off phase. The other electrodes are grounded except for one of them, which is used as a wall probe, operated either in I_{sat} or V_{fl} mode. The relevance of V_{fl} measurements is supported by tests performed with SLP which show good agreement between δV_{pl} and δV_{fl}. In a series of reproducible discharges, each of the electrodes (except for those used for the biasing) is alternately used as wall probe. The resulting 2D measurements of δV_{fl} and $\delta I_{sat}/I_{sat}$ are plotted in the left column of Fig. 5. In the right column, we plot the corresponding measurements in the HEXTIP plane. The measurements from the HEXTIP probe tips at the positions indicated by black dots in Fig. 5(b) are linearly interpolated to obtain the values on the flux tubes connected to each electrode. Measurements of δV_{fl}, Figs. 5(a) and 5(b), do not reveal strong differences in structure or absolute values in the two toroidally separated planes. In both cases, the δV_{fl} structure is shifted radially and vertically with respect to the biased electrodes. Further, we find $\delta V_{fl} \lesssim 4$ V in both planes. Good agreement is also found for relative changes in I_{sat},

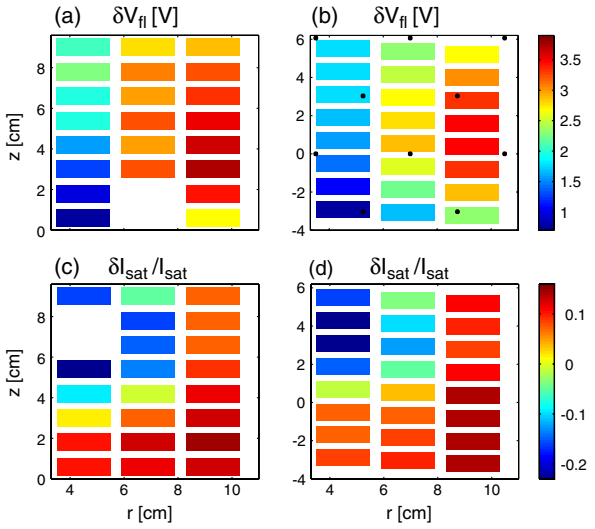

FIG. 5 (color online). (a), (c): Effects on V_{fl} and I_{sat} profiles due to the biasing, measured directly on the limiter. The square white area corresponds to the position of the electrodes that are used for the biasing. (b),(d): The same measurements, but obtained with HEXTIP, at 90° from the limiter. Measurements at the positions indicated by black dots in (b) are linearly interpolated to obtain the values on the flux tubes connected to each electrode.

Figs. 5(c) and 5(d). To cover an important fraction of the region where the largest changes of I_{sat} occur, a different set of electrodes is used for the biasing in this case. These measurements indicate that changes induced by the biased electrodes are fairly uniform along the magnetic field. High resolution measurements directly in front of the biased electrodes will be performed in the future to investigate the possibility of toroidally localized effects in this region.

These measurements show once more that the magnitude of the induced potential modifications in the plasma is well below the applied bias voltage. To further investigate this limitation, we have performed a scan in bias voltage between -40 V and $+40$ V applied to a pair of electrodes. This reveals that the I-V curve of the electrodes is strongly asymmetric, with a ratio of electron to ion saturation current of ≈ 30. Negative values of δV_{fl} measured with HEXTIP during negative bias are of very low amplitude ($|\delta V_{fl}| \lesssim 0.15$ V). For positive bias, a positive structure of δV_{fl}, similar to the one in Fig. 2(d) is observed. Its magnitude increases with applied bias voltage, is proportional to the electrode current and is limited to $\delta V_{fl} \lesssim 3.5$ V.

We interpret these observations within the model introduced in [23]. This assumes that the electrode current closes over a part of the limiter or vessel with a surface exceeding that of the electrode by a factor A. In the absence of cross-field currents, charge only flows along the magnetic field and $A = 1$. Assuming no potential variations along the flux tube (outside the sheaths), the electrode current is limited by the ion saturation current. To avoid large electron currents, the plasma potential therefore always stays above the potential at both of its endplates, and induced potential variations are approximately proportional to the bias potential when the latter exceeds $\approx T_e/e$. Such a proportionality can still persist when significant cross-field currents are present and $A > 1$ [23]. Induced potential variations saturate at high bias voltage only if A exceeds the ratio of electron to ion saturation current of an ideal LP. This is clearly the case in our experiments, indicating that a significant level of effective cross-field conductivity limits the achievable plasma potential modifications.

As seen in Fig. 2(d), the δV_{pl} structure is not centered around the flux tube where the bias is applied, but is shifted both upwards and radially outwards. This reveals a limit on the locality of the induced potential modifications, in addition to the limits on the magnitude of the potential variations discussed above. Comparing Figs. 2(b) and 2(d) suggests that the shift of the δV_{fl} structure occurs in the direction of plasma flows. Such behavior is also predicted from theoretical models [24,25]. To investigate the importance of flows for the location of induced potential modifications, we reverse the direction of the magnetic field, i.e., we set $B_\phi \rightarrow -B_\phi$ and $B_z \rightarrow -B_z$. In this case, the steady-state vertical $\mathbf{E} \times \mathbf{B}$ flow is reversed as well, such that it is now directed downwards at the LFS and upwards at the HFS of the I_{sat} profile. Figure 6(a) shows δV_{fl} for the bias applied in the blob region. White contours indicate the I_{sat} profile. In agreement with a vertical inversion of flows, δV_{fl} is now shifted downwards and radially outwards. Next, we change $|B_\phi|$ to radially move the plasma. This allows applying the biasing to regions with different plasma flows. In Fig. 6(b), $|B_\phi|$ is increased such that biasing is applied now to a region close to the peak of the I_{sat} profile, where no large flows are present. We observe a δV_{fl} structure that is rather well centered around the biased flux tube. In Fig. 6(c), $|B_\phi|$ is increased further and biasing is now applied to a region at the HFS of the I_{sat} profile, where the $\mathbf{E} \times \mathbf{B}$ flow is directed upwards. In agreement with the hypothesis that flows determine the position of the δV_{fl} structure, the latter is now shifted upwards.

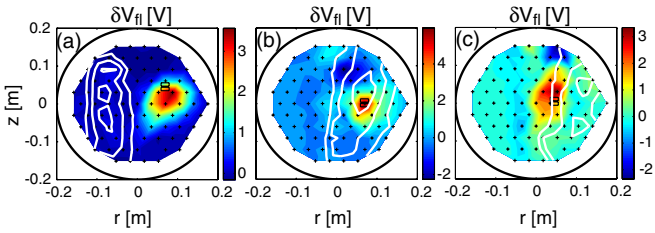

FIG. 6 (color online). δV_{fl} for plasmas with reversed field ($B_\phi, B_z < 0$) and $B_\phi = -75.6$ mT (a), $= -86.4$ mT (b), and $= -91.0$ mT (c). I_{sat} profiles are indicated by white contours.

To summarize, we have demonstrated the possibility of controlling blobs by creating convective cells using a 2D array of biasing electrodes that is installed on a metal limiter. The effect on time-averaged profiles induced by positively biasing a pair of electrodes reveals characteristics of a convective cell. Measurements on the limiter and over a cross-section toroidally displaced by 90° show that these perturbations are fairly uniform along the magnetic field. Using different biasing schemes, we have demonstrated the possibility of modifying both vertical and radial cross-field velocities of blobs. The magnitude of potential variations that can be achieved in the plasma is severely limited by cross-field currents. Furthermore, limitations on the locality of the effects associated with biasing have been revealed. The position of the induced potential modifications is shifted with respect to that of the biased flux tube in the direction of plasma flows.

This work is partly supported by the Fonds National Suisse de la Recherche Scientifique. We thank M. Gilmore and P. Ricci for helpful discussions and D. Lançon for helping with the installation of the electrodes.

[1] A. Loarte *et al.*, Nucl. Fusion **47**, S203 (2007).
[2] B. Lipschultz *et al.*, Nucl. Fusion **47**, 1189 (2007).
[3] S. J. Zweben *et al.*, Plasma Phys. Controlled Fusion **49**, S1 (2007).

[4] R. H. Cohen and D. D. Ryutov, Nucl. Fusion **37**, 621 (1997).
[5] J. Hara *et al.*, J. Nucl. Mater. **241–243**, 338 (1997).
[6] G. F. Counsell *et al.*, J. Nucl. Mater. **313–316**, 804 (2003).
[7] J. Stockel *et al.*, Plasma Phys. Controlled Fusion **47**, 635 (2005).
[8] S. J. Zweben *et al.*, Plasma Phys. Controlled Fusion **51**, 105012 (2009).
[9] A. Fasoli *et al.*, Plasma Phys. Controlled Fusion **52**, 124020 (2010).
[10] F. M. Poli *et al.*, Phys. Plasmas **15**, 032104 (2008).
[11] P. Ricci and B. N. Rogers, Phys. Rev. Lett. **104**, 145001 (2010).
[12] S. I. Krasheninnikov, D. A. D'Ippolito, and J. R. Myra, J. Plasma Phys. **74**, 679 (2008).
[13] D. A. D'Ippolito, J. R. Myra, and S. J. Zweben, Phys. Plasmas **18**, 060501 (2011).
[14] I. Furno *et al.*, Phys. Rev. Lett. **100**, 055004 (2008).
[15] I. Furno *et al.*, Phys. Plasmas **15**, 055903 (2008).
[16] C. Theiler *et al.*, Phys. Plasmas **15**, 042303 (2008).
[17] C. Theiler *et al.*, Phys. Rev. Lett. **103**, 065001 (2009).
[18] I. Furno *et al.*, Phys. Rev. Lett. **106**, 245001 (2011).
[19] C. Theiler *et al.*, Phys. Plasmas **18**, 055901 (2011).
[20] M. Podestà *et al.*, Phys. Rev. Lett. **101**, 045001 (2008).
[21] S. H. Müller *et al.*, Phys. Plasmas **12**, 090906 (2005).
[22] G. R. Tynan *et al.*, Phys. Rev. Lett. **68**, 3032 (1992).
[23] D. D. Ryutov, P. Helander, and R. H. Cohen, Plasma Phys. Controlled Fusion **43**, 1399 (2001).
[24] V. A. Rozhansky, A. A. Ushakov, and S. P. Voskoboynikov, Nucl. Fusion **39**, 613 (1999).
[25] A. Carlson, Phys. Plasmas **8**, 4732 (2001).